NeuroImage 285 (2024) 120482

Contents lists available at ScienceDirect

NeuroImage

journal homepage: www.elsevier.com/locate/ynimg

Intrinsic neural timescales relate to the dynamics of infraslow neural waves

Yujia Ao [a], Yasir Catal [a], Stephan Lechner [a,b,c], Jingyu Hua [d], Georg Northoff [a,*]

[a] Mind, Brain Imaging and Neuroethics Research Unit, Institute of Mental Health Research, Faculty of Medicine, University of Ottawa, Ottawa, ON, Canada
[b] Research Group Neuroinformatics, Faculty of Computer Science, University of Vienna, 1010 Vienna, Austria
[c] Vienna Doctoral School Cognition, Behavior and Neuroscience, University of Vienna, 1030 Vienna, Austria
[d] Department of Psychology, Faculty of Social Sciences, University of Ottawa, Ottawa, ON, Canada

ARTICLE INFO

Keywords:
Functional magnetic resonance imaging
Intrinsic neural timescales
Infraslow neural waves
Temporal input processing

ABSTRACT

The human brain is a highly dynamic organ that operates across a variety of timescales, the intrinsic neural timescales (INT). In addition to the INT, the neural waves featured by its phase-related processes including their cycles with peak/trough and rise/fall play a key role in shaping the brain's neural activity. However, the relationship between the brain's ongoing wave dynamics and INT remains yet unclear. In this study, we utilized functional magnetic resonance imaging (fMRI) rest and task data from the Human Connectome Project (HCP) to investigate the relationship of infraslow wave dynamics [as measured in terms of speed by changes in its peak frequency (PF)] with INT. Our findings reveal that: (i) the speed of phase dynamics (PF) is associated with distinct parts of the ongoing phase cycles, namely higher PF in peak/trough and lower PF in rise/fall; (ii) there exists a negative correlation between phase dynamics (PF) and INT such that slower PF relates to longer INT; (iii) exposure to a movie alters both PF and INT across the different phase cycles, yet their negative correlation remains intact. Collectively, our results demonstrate that INT relates to infraslow phase dynamics during both rest and task states.

1. Introduction

Think about being a surfer. You are surfing on a rough ocean. An adept surfer needs to adjust her/his surfboard to the peak, trough, rise, and fall of the ocean's ongoing waves to maintain her/ his balance. This is because the shape and speed of the waves vary across its different part of ongoing phase cycles. Most importantly, the surfer has to adapt her/ his movements to the ongoing dynamics of the ocean's wave, that is, especially its speed operating across different timescales (long, medium, short, etc.), in order to align and take advantage of the wave's power to propel the surfboard. Hence, the surfer is confronted with the rather challenging task of adapting her/his movements to the waves' ongoing phase dynamics while, at the same time, integrating the different timescales of the various waves.

Just like the ocean, the brain's neural activity is highly dynamic showing different waves which vary in their phases and timescales (Buzsaki and Draguhn, 2004; Golesorkhi et al., 2021b; Palva and Palva, 2018; Zuo et al., 2010). This is, for instance, manifest in the variation of its amplitude and its dynamic functional connectivity (FC), including so-called travelling waves, which speak to the spatial blood-oxygen-level-dependent (BOLD) propagation (Garrett et al., 2013; Gu et al., 2021; Raut et al., 2021; Shine et al., 2016). There is strong evidence that the dynamic FC is based on its underlying phases with their distinct positions or angles during the ongoing cycles of the infraslow neural waves, including the peaks, troughs, rises, and falls (Gutierrez-Barragan et al., 2019, 2022; Huang et al., 2017; Scheinost et al., 2016; Zhang et al., 2020). At the same time, the brain's neural waves operate on various timescales including shorter and longer ones, the so-called intrinsic neural timescales (INT) (Golesorkhi et al., 2021a, 2021b; Hasson et al., 2015; Himberger et al., 2018; Ito et al., 2020; Raut et al., 2020; Wolff et al., 2022; Yeshurun et al., 2021). How do the dynamics of the infraslow neural waves with their ongoing phase cycles relate to the INT? Like the surfer, the brain is confronted with the challenge of integrating and connecting the wave dynamics of its ongoing phase cycles with its various timescales, the INT. Hence, addressing this yet open question is the goal of our study. This will provide insights into how two key components of the brain's neural activity, namely phase dynamics and INT, are related to each other and integrate their distinct timescales, e.g., shorter (phase dynamics) and longer (INT). That, in turn, is key for our understanding of higher-order

* Corresponding author at: Mind, Brain Imaging and Neuroethics, Institute of Mental Health Research, University of Ottawa, 1145 Carling Avenue, Room 6435, Ottawa, ON K1Z 7K4, Canada.
E-mail address: georg.northoff@theroyal.ca (G. Northoff).

https://doi.org/10.1016/j.neuroimage.2023.120482
Received 21 September 2023; Received in revised form 23 November 2023; Accepted 1 December 2023
Available online 2 December 2023

cognitive features like consciousness (Northoff and Huang, 2017) and self (Wolman et al., 2023) where the integration of different timescales is a core feature.

Previous research on neural waves and their phase cycles predominantly focused on the faster frequency range of 1–80 Hz including so-called Theta (4–8 Hz), Alpha (8–12 Hz), Beta (12–40 Hz), and Gamma (40–Hz) waves in Electroencephalography/Magnetoencephalography (EEG/MEG) studies (Adaikkan et al., 2019; Helfrich et al., 2018; Hua et al., 2022; Klimesch et al., 2007). The ongoing waves' phase dynamics are here measured and operationalized by frequency sliding (Cohen, 2014). As shown in Fig. 1, the frequency sliding method calculates the temporal derivative of the phase angle for a filtered signal, thus measuring the sliding of the instantaneous frequency during a given time series, the so-called peak frequency (PF) for each time point (Cohen, 2014). Hence, PF measuring the speed of phase-angle-based changes over time, can, more generally, be conceived as an index of the dynamics of neural waves. Subsequent research has demonstrated PF's predictive ability for visual perception (Samaha and Postle, 2015), its reflection of temporal integration and segregation (Wutz et al., 2018), and its influence on task performance (Benwell et al., 2019) including thoughts (Hua et al., 2022). Moreover, abnormalities in PF have been observed in depression (Wolff et al., 2019). Together, these findings suggest a key role for phase dynamics of waves and specifically their speed in the brain's information processing including its cognition.

The infraslow neural waves, within the 0.01–0.1 Hz range in functional Magnetic Resonance Imaging (fMRI), have increasingly been recognized for their importance in the complex neural stochastic processes of integration and segregation (Golesorkhi et al., 2021b; Wolff et al., 2022). This recognition is evident in various studies (Ao et al., 2022; Doucet et al., 2012; Gong and Zuo, 2023; Thompson and Fransson, 2015), encompassing research on consciousness (Huang et al., 2014), cognitive processes (Palva and Palva, 2012), and mental disorders (Scalabrini et al., 2020). Unlike in EEG/MEG, fMRI investigations into infraslow neural waves and their phase dynamics have only begun recently (Bolt et al., 2022). Current fMRI studies have underscored the significance of wave-like dynamics featured by its phase as a foundational aspect of understanding the brain's spatiotemporal structure (Pang et al., 2023, 2021; Raut et al., 2021). While other studies demonstrated the modulation of specific brain activation and coactivation patterns during various phases, including peak, trough, rise, and fall in the infraslow frequency domain of fMRI (Gutierrez-Barragan et al., 2019; Huang et al., 2017; Scheinost et al., 2016; Wang et al., 2019). Despite these advances, our comprehension of wave dynamics across different phases (peak, trough, rise, fall) in the domain of the brain's infra-slow frequency fluctuations remains somewhat limited. Specifically, the wave dynamics of infraslow frequency fluctuations with potentially differential roles of peak/trough and rise/fall components during the ongoing phase cycles including their topographic distribution remain yet unclear. Hence, our first main aim is to address this gap in our knowledge of the dynamics of neural waves in the infraslow frequency domain of fMRI.

In addition to its phase dynamics, the brain's neural activity can also be characterized by different timescales, the so-called intrinsic neural timescales (INT). Prior research has suggested a hierarchy of INT—ranging from short to long—as measured by the autocorrelation window (ACW) (Golesorkhi et al., 2021a, 2021b; Ito et al., 2020; Raut et al., 2020; Wolff et al., 2022). This measure estimates the decay rate of the autocorrelation function, a signal's correlation with itself at different time lags, and is considered a key mechanism for matching input stochasticity with ongoing temporal statistics (Hasson et al., 2015; Wolff et al., 2022). Given that the phase dynamics may operate at different timescales through its speed (PF), one may want to raise the following question: Are the brain's INT and thus its ACW related to the ongoing wave dynamics, its speed, as measured by PF? Two recent EEG studies demonstrate a correlation of ACW with PF and inter-trial phase coherence including their breakdown in pathological processes, e.g., schizophrenia (Lechner and Northoff, 2023) and loss of consciousness in anesthesia (Buccellato et al., 2023). This underscores the relevance of the relationship of INT and ACW in the faster frequencies (1 to 80 Hz) of traditional cognitive information processing. Does the same hold for the infraslow frequency domain (0.01 to 0.1 Hz) and their topographies in fMRI? Probing the relationship of ACW and PF in the infraslow frequency domain is the second main aim of our study.

In this study, we first analyze the HCP 3T resting-state data to investigate the PF across different phases and to explore how the distinct components during the ongoing phase cycles modulate PF. Previous findings have noted varied brain activations in different phases of peak, trough, rise, and fall, indicating that infraslow wave dynamics vary with phase cycle changes (Huang et al., 2017; Wang et al., 2019). We subsequently hypothesize that the magnitude of PF is phase-specific and is modulated by the phase cycle, e.g., peak, trough, rise and fall. Next, we aim to examine the relationship between PF and INT. Based on previous

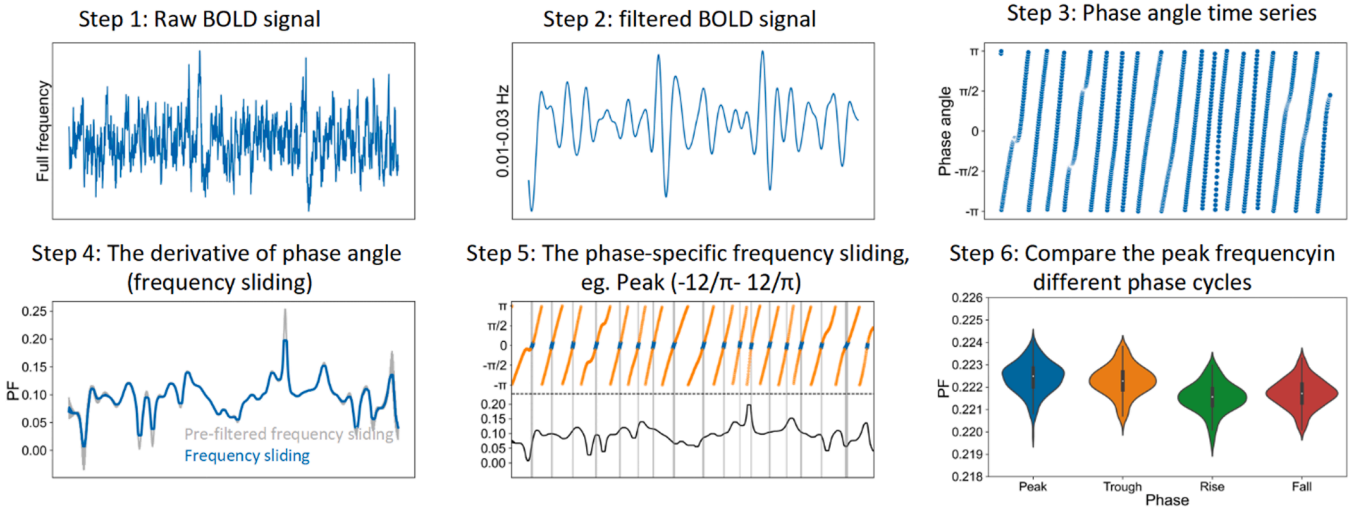

Fig. 1. Schematic representation of the frequency sliding method (Cohen, 2014). Step 1: Initiate with the raw BOLD signal. Step 2: Filter the raw data into four narrow bands: 0.01–0.03 Hz, 0.03–0.05 Hz, 0.05–0.07 Hz, and 0.07–0.09 Hz. Step 3: Determine the phase of the filtered data. Step 4: Calculate the temporal derivative of the phase angle time series, representing PF. Step 5: Extract the PF time series for distinct phases and compute the average of PF within each phase cycle (the Figure exemplifies a "peak" scenario, as the shade shows). Step 6: Conduct statistical comparisons of PF across various phases, including peak, trough, rise, and fall.

findings (Buccellato et al., 2023; Lechner and Northoff, 2023) of their negative relationship in EEG, we expect the same direction in their correlation in the infraslow frequency domain of fMRI, that is, longer ACW corresponds to slower PF. Lastly, we investigate how PF including its modulation by the ongoing phase cycles and INT change during a movie-watching task. Even though no prior fMRI studies focused on the task-related changes of spontaneous phase dynamics as measured by PF, changes in the dynamics of phase synchrony patterns (Alderson et al., 2020; Stark et al., 2020) and phase-specific performance in peak, trough, rise and fall (Wang et al., 2019) have been reported during task states. Thus, we hypothesize that the PF shows phase-specific changes during task states; we especially expect that the task-related changes in PF occur across the whole brain, e.g., from unimodal to transmodal cortical regions, as the movie stimuli involve both sensory and cognitive functions (Kringelbach et al., 2023; Rajimehr et al., 2022).

2. Results

2.1. Infraslow phase dynamics (peak frequency/PF) varies in different phase components and frequency bands

Our initial evaluation involved probing the similarity between the EEG-based frequency sliding methods of Cohen (2014) and Lechner and Northoff (2023) in the infraslow frequency range of fMRI. All of the R values obtained for the four frequency bands exceeded 0.9, thereby suggesting that our method can be corroborated by different methodologies (Supplementary Fig. 2).

The specific analysis is illustrated in Fig. 1, step 5 and 6. To maximize the difference of PF across different phases, we calculated the average PF values across four narrow phase windows with 30° for each, resulting in topographies at the group level for peak (-15°∼15°), trough (165°∼180° & -180°∼-165°), rise (-105°∼-75°), and fall (75°∼105°) phases, in line with previous studies (Huang et al., 2017; Wang et al., 2019). To quantify the spatial similarity of PF topographies across the four bands, we correlated each region between each pair of bands, as depicted in

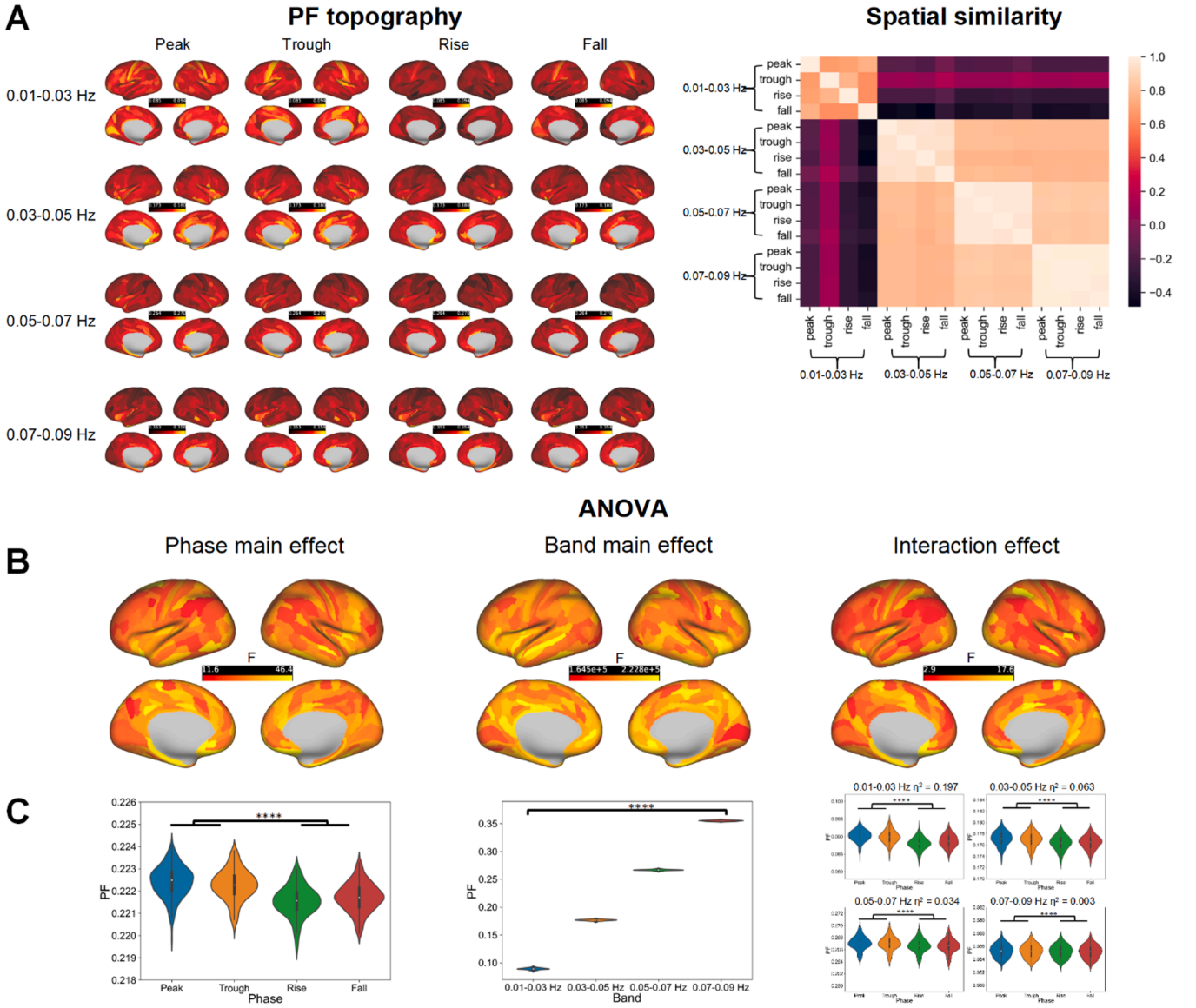

Fig. 2. PF across four bands and phases. (A) Left: The brain maps of PF within different filtered bands and phases. Right: Correlation matrix of each pair of topographies (B) The ANOVA outcomes for brain regions in Glasser's atlas. (C) The comprehensive post-hoc analysis was conducted at the whole-brain level. (For interpretation of the references to colour in this figure legend, the reader is referred to the web version of this article.)

Fig. 2(A). A notable observation was the low similarity between the 0.01–0.03 Hz band and higher bands during the phase cycles (r = -0.48∼0.16). However, strong within-band and between-phase correlations were evident (r = 0.62∼0.98). This indicates that the very slow frequency band possesses a unique spatial topography.

We next conducted a 2-way within-subject ANOVA for frequency sliding across different phases and bands, as shown in Fig. 2. Fig. 2(B) illustrates FDR-corrected brain maps with significant F-values (P < 0.05). The results suggest higher PF during peak and trough phases while lower PF during rise and fall phases were observed across most brain regions (Fig. 2(C), F = 820.6, P < 0.0001). PF appears to increase with the increase of the frequency band when applying different band passes (F = 1.40e + 06, P < 0.0001). This is further supported statistically as we detected a robust interaction (F = 250.1, P < 0.0001) between phase/PF and bands, characterized by lower phase differences at higher frequencies, as reflected in the decreasing effect size.

In sum, these findings suggest that PF is higher during peak and trough but lower during rise and fall. This effect is most prominent in the 0.01–0.03 Hz band, which displays a unique spatial topography while this effect diminishes in faster frequency bands. These results were consistently replicated using 7 T resting-state data, as illustrated in Supplementary Fig. 3. In contrast, while the ANOVA result is significant in 0.01–0.03 Hz, low effect size/no significant differences between peak-trough and rise-fall phases were observed in the surrogate data, as shown in Supplementary Fig. 4. This further supports the validity of the peak-trough and rise-fall phase differences in terms of their peak frequency as an intrinsic feature of the spontaneous activity's temporal structure.

2.2. PF is modulated by the distinct components of the ongoing phase cycles

We have so far demonstrated that PF varies across four phases. To examine the effects of the distinct components of the ongoing phase cycles on PF, we segmented the phase into narrow bins using a window length of 30 degrees and a step length of 1 degree. This process resulted in 360 narrow phase bins (-180∼-150, -179∼-149, and so on), and we calculated the mean PF in each bin. We computed the normalized Kullback–Leibler (KL) divergence against a uniform distribution, a classical index to measure the modulation effect (Helfrich et al., 2018; Tort et al., 2010), to quantify how strongly the PF distribution was modulated by the different phase components.

In agreement with the results above, the magnitude of PF is higher during the peak and trough phases and lower during the rise and fall phases (Fig. 3(A)). We further applied within-subject ANOVA for each region and the average of them. Interestingly, the ANOVA and post-hoc results show that KL divergence significantly decreases as the frequency of the band increases (F = 657.5, P < 0.0001, Fig. 3, left), suggesting that the very slow frequency, 0.01–0.03 Hz, exhibits the strongest modulation effect. Topographical analysis reveals that this slow-fast frequency difference is significant in the whole brain (FDR corrected, Fig. 3(C)). This observation is replicated using 7 T resting-state data, as shown in Supplementary Fig. 5. In contrast, the surrogate data display a much lower modulation index while no similar pattern was observed (Supplementary Fig. 4). This supports the assumption that the peak frequency differences between the different phase components are an intrinsic feature of the temporal structure of the brain's spontaneous activity.

2.3. Relationship between phase dynamics (PF) and timescales (ACW)

As delineated in Fig. 4(A), the ACW is longer in the Default Mode Network (DMN) but shorter in visual and sensorimotor regions. This pattern reflects segregation between unimodal and transmodal regions, an observation that aligns with previous studies (Golesorkhi et al., 2021a, 2021b; Huntenburg et al., 2018; Margulies et al., 2016).

To investigate the relationship of ACW with PF, we computed the spatial similarity between PF in the four bands (0.01–0.03 Hz, 0.03–0.05 Hz, 0.05–0.07 Hz, and 0.07–0.09 Hz) and ACW for 0.01–0.1 Hz. The correlation analysis between the mean of PF and ACW demonstrated a consistently significant negative trend across all bands (R = -0.22, -0.84, -0.79, -0.76, with all P-values <0.0001): The longer

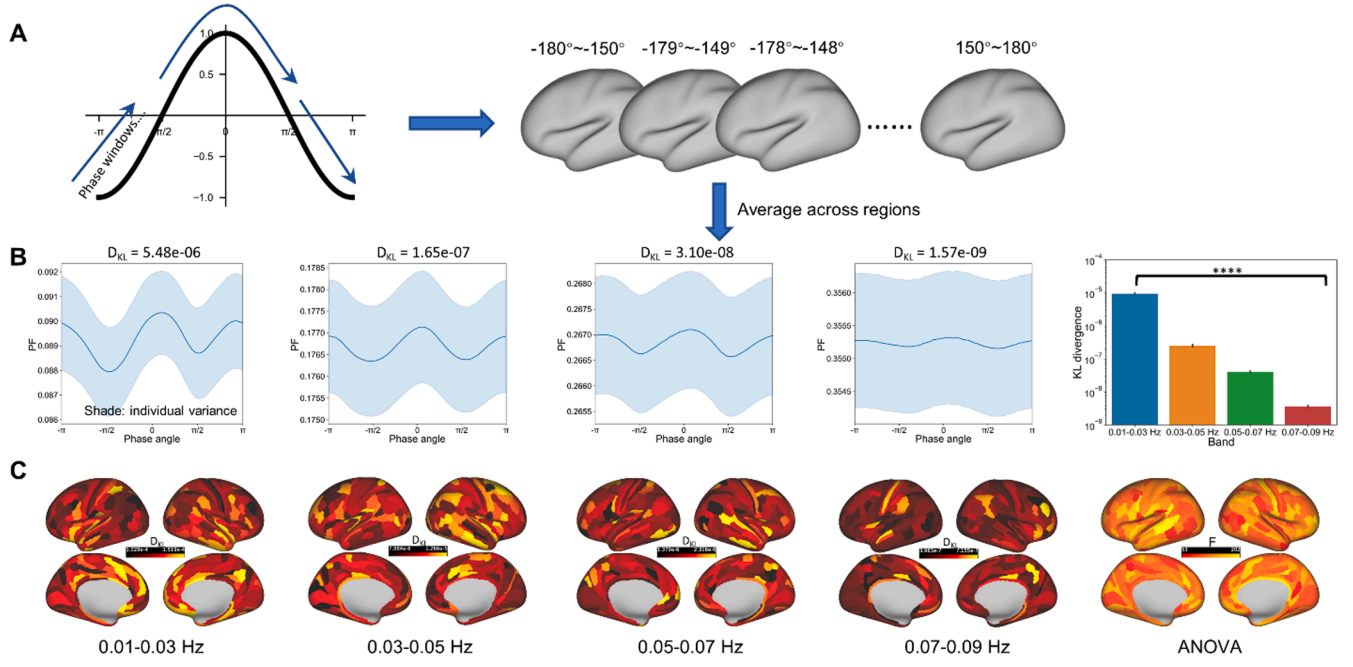

Fig. 3. Phase modulation effects on PF. (A) The schematic figure illustrates the method to calculate PF in each phase bin (B) Line charts: The blue line represents PF within the phase cycle, ranging from -π to π, with the shaded area denoting the standard deviation of individual variances. Bar chart: The ANOVA results for KL divergence across the four frequency bands. (C) Topographies of KL-divergence and ANOVA result. (For interpretation of the references to colour in this figure legend, the reader is referred to the web version of this article.)

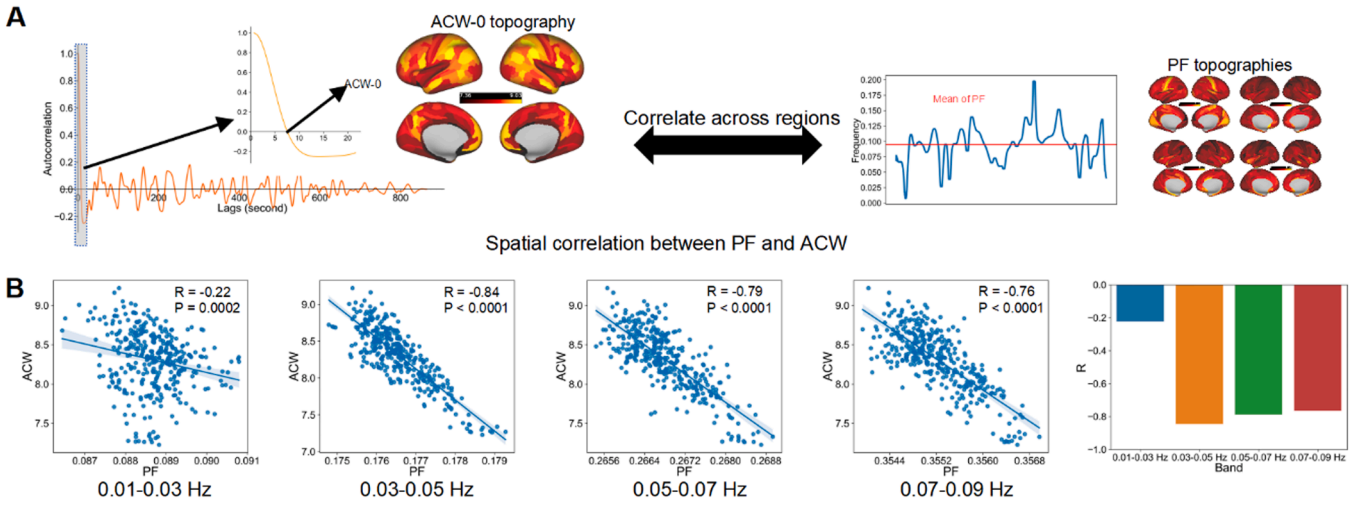

Fig. 4. Relationship between PF and ACW. (A) A graphical representation illustrating the process of calculating the correlation between ACW and PF. (B) The regression plot depicts the relationship between ACW and PF across four frequency bands, each dot represents each brain region. The accompanying bar chart highlights the differences in Pearson's correlation coefficients across the four bands.

the INT/ACW, the lower the PF in the same region. These results were replicated using the 7 T data, as indicated in Supplementary Fig. 6.

We further checked the correlation between frequency power and ACW (Supplementary Fig. 7). The correlations between frequency power and ACW are significantly lower than that between PF and ACW in four bands (Z = 2.11, 11.49, 8.80, 9.37, all of P values <0.05). This suggests that the ACW is, in part, related to specifically the nonlinear component of the signal as reflected in the phase angle of the PF as that is eliminated in frequency power.

In phase-shuffled surrogate data, PF-ACW correlations maintain almost the same with actual data in 0.03–0.05 Hz, 0.05–0.07 Hz, 0.07–0.09 Hz (see Supplementary Fig. 8, Z = -0.24, -0.25, -0.00, all of P values >0.05). This is not surprising given that the phase cycles with their distinct components themselves, although temporally randomized in their timing, are essentially preserved in the phase-shuffled surrogate data. This distinguishes the result from the frequency power where the phase components themselves like peak and trough are no longer preserved as the modulus of the Hilbert signal is taken. The fact that only the frequency power but not the phase-shuffled surrogate data impaired the correlation of PF with ACW suggests that the nonlinear phase components themselves like peak and trough, but not so much their exact timing, drive their relationship with ACW.

Note that the correlation between ACW and PF shifts to a positive one in the 0.01–0.03 Hz band (Z = 5.18, P < 0.0001). Given that our shuffling method, i.e., shuffling the sequency of Fourier phase, specifically eliminated the nonlinearity component of the phase dynamics while preserving the amplitude characteristics, this suggests that the negative relationship of PF and ACW is partly explained by nonlinearity rather than linear features of the signal in the very slow band of 0.01–0.03 Hz but not so much in the more linear features of the faster bands. This is in line with our findings in Fig. 2 and previous findings on infraslow neural oscillations (Buzsáki and Draguhn, 2004; Zuo et al., 2010), that 0.01–0.03 Hz corresponding to Slow-5 (0.01–0.027 Hz) contains unique feature with a higher frequency corresponding to Slow-4 (0.027–0.073 Hz).

2.4. Effect of band-passing

To mitigate the potential influence of filtering edge effects, we expanded our analysis to replicate the studies using different band-passing filters like 0.005–0.01 Hz as well as 0.01–0.03 Hz as being analyzed within a filtered band of 0.005–0.1 Hz. This supplemental analysis yielded results that concurred with the primary analysis (as delineated in Figs. 2–4 and Supplementary Fig. 9); this suggests that the outcomes of our study are not merely artifacts of edge effects. Note also the even steeper negative correlation of ACW and PF in this broader bandpass; this is in line with the observation that the length of the ACW is strongly shaped by the slower components of the frequency spectrum (Honey et al., 2012; Zilio et al., 2021).

2.5. Task-modulation of infraslow phase dynamics (PF)

The task leads to higher PF in the trough phase than in the peak when compared to the resting state (as shown in Fig. 5(A), left). The simple effect test indicated that this difference was significant only at 0.01–0.03 Hz (T = -22.22, P < 0.0001, Fig. 5(A), right). Moreover, the task-state KL divergence in 0.01–0.03 Hz exceeded that observed during the resting state (T = -6.86, P < 0.0001, Fig. 5(C)). Topographical analysis the KL divergence increased mainly in visual, auditory, and sensorimotor cortices which, presumably, are related to the processing of the external sensory stimuli during the movie-watching task.

These findings led us to hypothesize that this increased KL divergence during the task state (compared to rest) is primarily driven by the difference between peak and trough during the task state. To investigate this, we compared PF between resting and task states in different phases at 0.01–0.03 Hz using a paired t-test. We noted a decrease in PF during the task state (compared to rest) across all phases. Topographical analysis shows that this PF decrease is largely present in visual, auditory, and sensorimotor cortices, which is consistent with the KL divergence results. Notably, the effect size of the difference between rest and task was greatest in the peak, while it was smallest in the trough. This observation suggests that the increased phase modulation in the task state is primarily driven by the change in the relationship of peak and trough when compared to the resting state (Fig. 5(A), left).

Several studies have indicated that resting-state and task-related brain activities may be associated with different frequency components beyond the infraslow range (Chen and Glover, 2015; Palva and Palva, 2018). For instance, higher frequencies, such as Slow-3 (0.073–0.198 Hz), have been shown to have specific effects in resting-state and cognitive functions (Ao et al., 2023; Wang et al., 2020; Zhang et al., 2022). In our study, we further examined the differences in PF during rest and task conditions across a broader frequency range of 0.01–0.2 Hz. As demonstrated in Supplementary Fig. 10, we observed frequency-specific effects across various narrow bands. Notably, task modulation was predominantly observed in the 0.01–0.1 Hz range, particularly within the 0.01–0.03 Hz band. This suggests that the

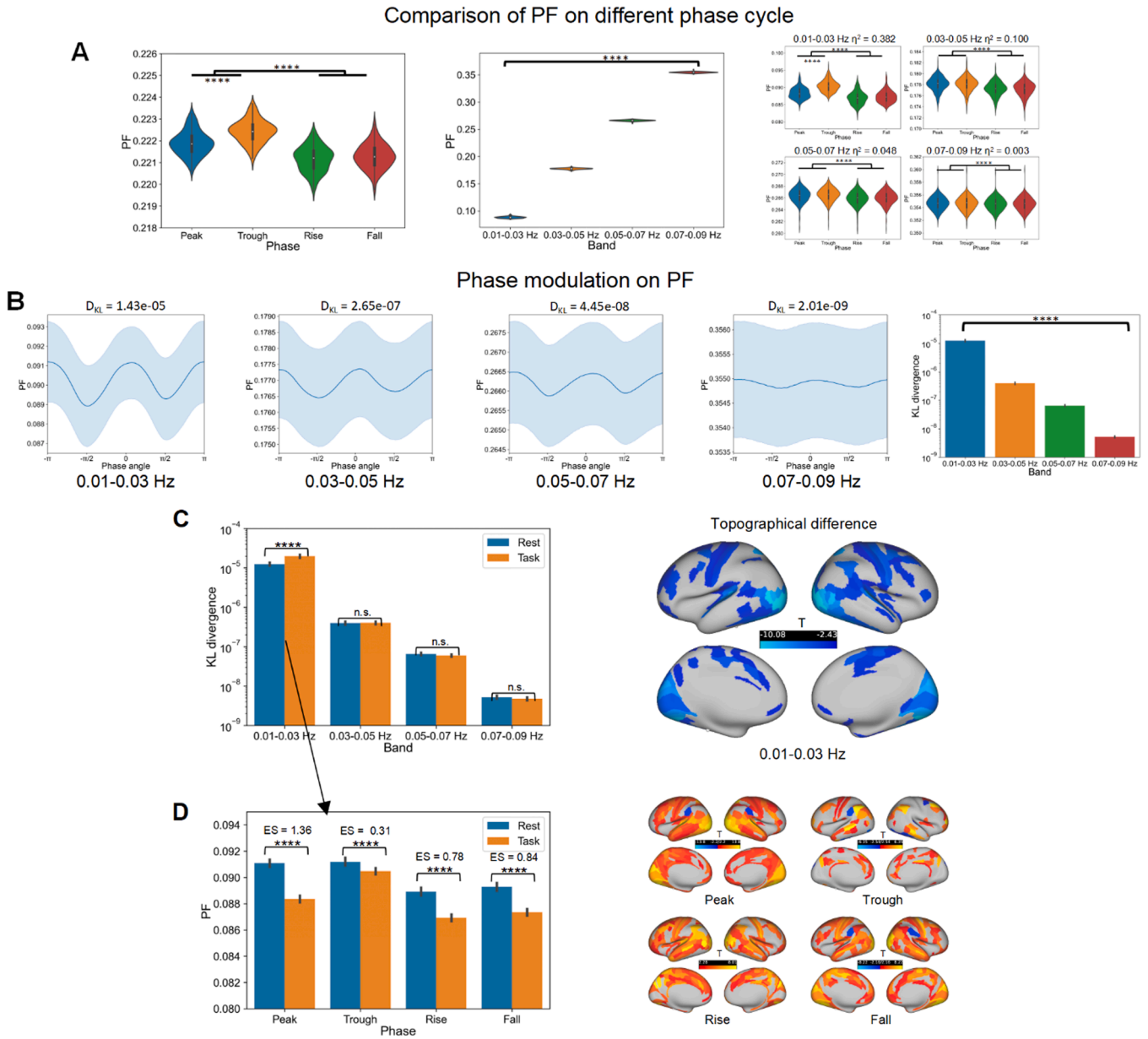

Fig. 5. Task-state data analysis. (A) Comparison of PF on different phase cycles corresponding to Fig. 2. (B) KL divergence analysis corresponds to Fig. 3. (C) Left: Rest-task difference of KL divergence at 4 bands. Right: Rest-task topographical difference of KL divergence at 0.01–0.03 Hz. (D) Left: Rest-task difference of PF in 4 phases at 0.01–0.03 Hz. Right: Rest-task topographical difference of PF at 4 phases.

infraslow component is particularly significant in the context of a naturalistic continuous task like our movie-watching task.

2.6. The relationship between phase dynamics (PF) and INT (ACW) during the task state

We next investigated the relationship between phase dynamics (PF) and INT (ACW) during the task state. First, we correlated PF and INT during the task state. Consistent with the resting-state data, the correlations are significantly negative across all four sub-bands (R = -0.54–-0.20, $P < 0.0001$, Fig. 6(A)). Both decreases and increases in ACW length during the task state were observed relative to the resting state. Specifically, in visual and auditory cortices, regions that play vital roles in processing movie stimuli, we observed an increase in ACW length during task-related activity compared to the resting state. Conversely, the ACW length in the sensorimotor cortex, the posterior cingulate cortex, and the prefrontal cortex decreased during the task state compared to the resting state (Fig. 6(B)).

Lastly, we calculated the spatial correlation between the unthresholded rest-task difference topographies of PF and ACW. As in the resting state, the correlation consistently shows a negative relationship between PF and ACW, providing yet further evidence that the task modulates the topographies of both PF and ACW in somewhat analogous ways (Fig. 6(C)).

3. Discussion

Utilizing the Human Connectome Project's (HCP) 3T/7T dataset, we, operating in the infraslow frequency domain, investigated the spontaneous phase dynamics of neural waves, their association with INT, and the subsequent changes during a movie-watching task.

Our first main finding consists of the observation that the speed of the infraslow neural waves, quantified by PF, exhibits higher values at peak/trough and lower values at rise/fall. This modulation of the phase

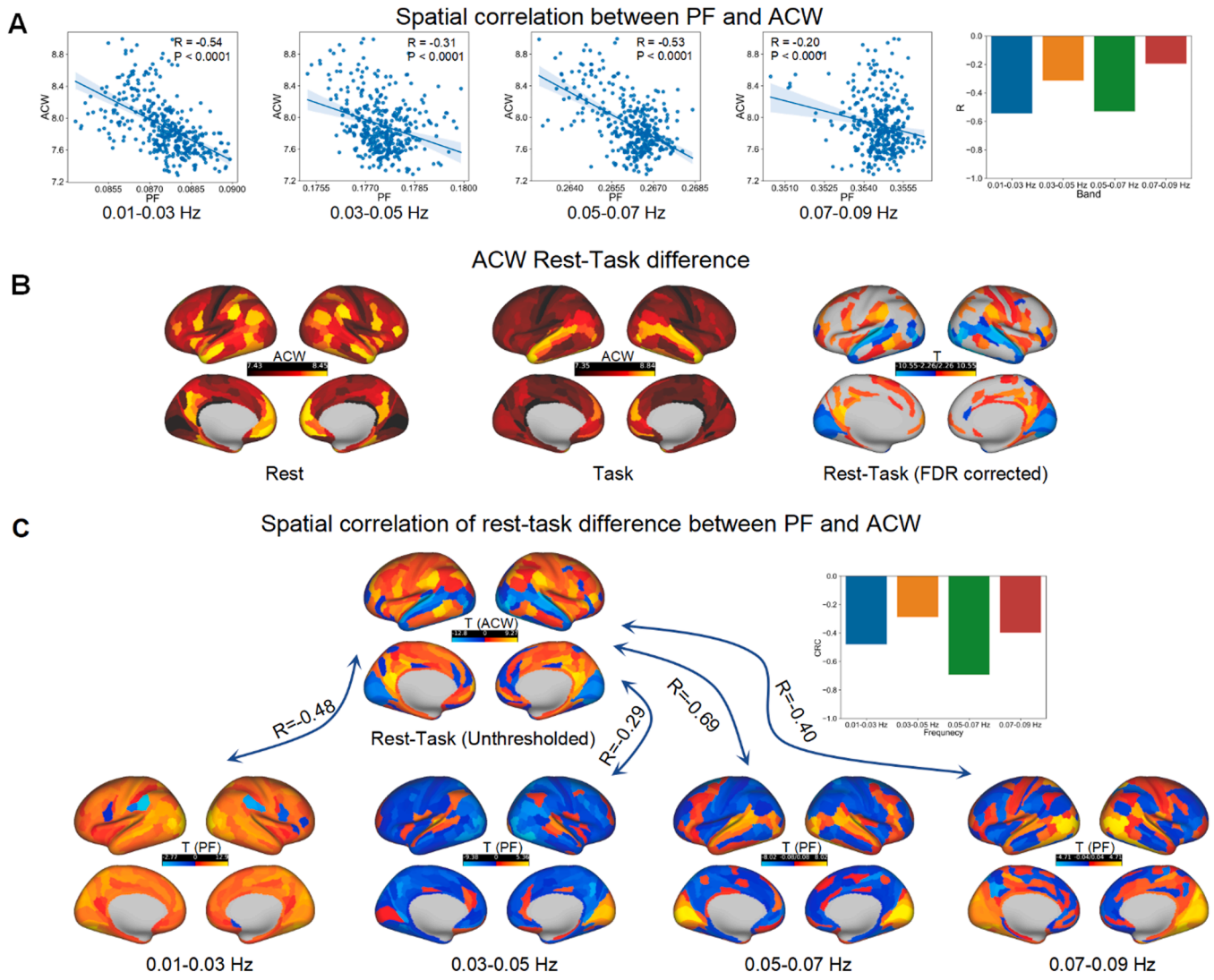

Fig. 6. ACW rest-task difference. (A) Spatial correlation between PF and ACW in task state. (B) Left: ACW topography in resting state. Middle: ACW topography in task state. Right: T-test topography of rest-task ACW. (C) Top: Unthresholded rest-task difference of ACW. Below: Unthresholded rest-task difference of PF in four bands.

cycle, ranging from -180° to 180°, is clearly illustrated in Fig. 3. Significantly, this effect is notably present within the 0.01–0.03 Hz band, a very slow frequency range, while it is weaker in faster frequency ranges. During the task state, the modulation effect of the phase cycle on PF intensifies within the 0.01–0.03 Hz band. Intriguingly, despite a consistent increase in PF across four phases from rest to task, this stronger modulation effect is primarily driven by a heterogeneous increase in PF at peak and trough positions.

The second main finding consists of the negative correlation between PF and INT, corroborating the findings of the Buccellato et al. (2023) EEG study. While we noted task-related changes in PF and ACW, we also demonstrated the persistence of their negative correlation during the task state. In sum, we demonstrate the major role of the brain's ongoing infraslow wave dynamics including its relation to INT in shaping neural activity during both rest and task states.

3.1. *Wave dynamics and its task modulation*

Neural activities exhibit substantial temporal variations and dynamism (Kringelbach and Deco, 2020). Our research illustrates that PF, a measure of the speed of neural waves, varies concurrently with phase cycle changes. Within resting-state data, we observed higher PF values at peak/troughs and lower PF values during rise/fall across all brain regions. These findings demonstrate the importance of the ongoing phase cycles in shaping the dynamics, that is, the speed of neural activity.

Previous resting-state fMRI studies have identified distinct brain states as configured by the phase of global brain activity during peak, trough, rise, and fall stages (Gutierrez-Barragan et al., 2019; Scheinost et al., 2016). Yet, the task-related modifications of these phase-dependent brain states remain underexplored. Our study pioneers an examination of wave dynamics in the infraslow frequency domain including task state modulations. We found that PF decreases in the task state, suggesting a slowing of wave speed in response to movie stimuli. The slower speed potentially enables the brain to incorporate and integrate the shorter micro-contents into longer macro content providing psychological continuity, coherence, and unity of the movie in our perception (Himberger et al., 2018). Concurrently, we observed an increase in phase modulation during the task state, suggesting a broader range of timescales operating across different phases which, as we speculate, may be related to the encoding and processing of the movie's different timescales (Golesorkhi et al., 2021b; Wolff et al., 2022). Interestingly, despite a consistent decrease in PF across the ongoing phase cycles, the reduction is most significant at the peak and minimal at

the trough, largely maintaining fast speed at the trough. Given that slow PF and longer INT may allow for temporal integration of inputs while faster PF with shorter INT favors their temporal segregation (Hua et al., 2022; Wolff et al., 2022), we suppose that the task-related modulation of PF and INT allows for the concurrent integration and separation of the movie's different timescales: while movie inputs related to each other over longer stretches of time necessitate slower activity (as through the lowering of PF at the peak) for their temporal integration, faster activity (through the preservation of higher PF at the trough) persist in processing the fast-changing movie contents concurrently.

Our results highlight the significant and strongest effect of the 0.01–0.03 Hz band on phase dynamics and task-related changes. The function and role of this frequency band, labeled Slow-5 within the infraslow frequency range (Buzsáki and Draguhn, 2004; Wang et al., 2020; Zuo et al., 2010), remains poorly understood compared to the higher frequency oscillations, such as theta and alpha bands. Our findings propose that the Slow-5 wave may play a pivotal role in both spontaneous dynamics and the encoding of external stimuli, corroborating several fMRI studies (Gutierrez-Barragan et al., 2019; Han et al., 2011; Raut et al., 2021). For instance, Gutierrez-Barragan et al. found that the power spectral density of brain coactivation patterns and the global signal peak at approximately 0.02 Hz, suggesting that brain states are modulated by the ongoing phase dynamics within the 0.01–0.03 Hz range (Gutierrez-Barragan et al., 2019). This may include also body-based physiological modulation as Raut et al. identified a broad peak of coherence at 0.025 Hz between physiological signals (including respiration, heart rate, and pupil size) and network signals (Raut et al., 2021). Collectively, we propose that the 0.01 to 0.03 Hz band may harbor unique and vital information about brain-body coupling that strongly modulates spontaneous brain activity and its temporal encoding of the body's continuous inputs to the brain, a hypothesis that merits further investigation.

3.2. Wave dynamics relate to the INT

Our study reveals a negative correlation between the speed of wave dynamics (PF) and the length of INT. This observation aligns with expectations that a slower oscillation corresponds to a longer intrinsic timescale (Honey et al., 2012; Zilio et al., 2021). Such an outcome reaffirms the empirical findings from an EEG study investigating conscious states (Buccellato et al., 2023). Interestingly, that EEG study reported a disruption of the negative PF-ACW correlation in unconscious states. This provides additional evidence for the intrinsic cross-scale temporal organization of wave dynamics and INT. Given that both wave dynamics and INT are known to reflect the brain's inherent capacity to encode inputs (Golesorkhi et al., 2021b; Samaha and Postle, 2015) including their temporal integration and segregation (Wolff et al., 2022; Wutz et al., 2018), we propose that this cross-scale intrinsic temporal relationship may be crucial for processing complex stimuli featured by a variety of different timescales like in a movie.

An interesting observation is the strengthening of the negative correlation between PF and ACW when the low cut-off bandpass is reduced from 0.01 to 0.005. This finding implies that the negative relationship between PF and ACW is predominantly influenced by the very slow frequencies. Although previous research has investigated ACW in both the low-frequency range in fMRI (Ito et al., 2020; Raut et al., 2020) and the high frequency in EEG/MEG (Golesorkhi et al., 2021a; Wolman et al., 2023; Zilio et al., 2021), no study has examined the frequency-sensitivity of ACW. As our study shows that slower to faster PF are associated with distinct components within the ongoing phase cycles, we suggest that the intrinsic timescales in sub-frequency bands should be considered.

3.3. Limitation

Our study primarily utilizes resting-state and movie-watching fMRI data. While movie-watching is a natural continuous stimulus that shows distinct modes of brain function (Demirtaş et al., 2019; Finn and Bandettini, 2021; Huk et al., 2018), it differs from traditional cognitive tasks in its continuous stimulus presentation rather than discontinuous stimuli as in typical event-related paradigms (Huk et al., 2018), for which reason it does not involve behavioral responses. This distinction is important to note, as our findings regarding PF-ACW correlations are derived under this specific condition of a continuous naturalistic task paradigm. Hence, future research on the PF-ACW relationship in more discontinuous typical event-related paradigms is warranted. Moreover, the lack of direct behavioral measures in our dataset limits our ability to draw definitive conclusions about the cognitive functionalities of wave dynamics and INT in more varied or specific cognitive tasks. Future research should aim to include a broader range of cognitive tasks including continuous and discontinuous with corresponding behavioral response data to better understand and apply these findings in cognitive neuroscience.

A further limitation of our study is the use of a dataset from the HCP comprising solely healthy subjects. Given that wave dynamics and ACW reflect the individuals' ability to process inputs, exploring individual differences in pathological or other extreme states could provide valuable insights into future research. Studies should consider including different groups of subjects, such as those experiencing brain aging or mental disorders, to better examine the behavioral and functional relevance of wave dynamics and INT.

Lastly, our analysis was conducted at the conventional infraslow frequency of 0.01–0.1 Hz, primarily to develop a method for studying the dynamics of neural waves in fMRI data. Considering that important neural information is also contained in higher frequencies (>0.1 Hz) (Buzsáki and Draguhn, 2004; Chen and Glover, 2015; Zuo et al., 2010), future research should investigate wave dynamics in higher frequencies using open band passes (Sasai et al., 2021; Wang et al., 2020). This would provide a more comprehensive understanding of phase dynamics and INT across the whole frequency spectrum of timescales from longer to shorter.

3.4. Conclusion

Visualize yourself as a surfer riding the neural waves of the brain. Our findings indicate that the speed of these neural waves varies across their peaks, troughs, rises, and falls, mirroring the changing conditions a surfer faces on the waves of the ocean. Importantly, the length of intrinsic neural timescales requires adaptable responses, similar to a surfer adjusting to the ongoing and continuously changing wave patterns. Furthermore, an adept surfer should always be ready to respond to unexpected changes, analogous to the way the movie task changed both wave dynamics and INT. Based on our research, we propose that wave dynamics and their relationship to the INT play a pivotal role in organizing the temporal features of the brain's information processing. Future research should further investigate how specific cognitive processes and individual differences influence wave dynamics and INT. Lastly, the development of effective clinical interventions and therapies, aimed at "mastering the neural waves", should be considered within the context of the temporospatial approach of the brain-mind connection that recently has been introduced, e.g., Spatiotemporal Neuroscience (Northoff et al., 2020a, 2020b).

4. Methods

4.1. Data acquisition

The study utilized the fMRI dataset from Human Connectome Project (HCP) S1200 release (Van Essen et al., 2013). A total of 179 subjects with comprehensive scan data from both 3T and 7T imaging were incorporated. The 3T dataset was applied for the resting-state analysis, while the 7T data was employed for replication and task analysis. The

participants' ages span from 22 to 35 years, with 108 female participants.

The 3T resting-state data collection was performed over two consecutive days. On each day, each participant underwent two 15-minute runs, resulting in four resting-state scans per participant (rfMRI_REST1_LR, rfMRI_REST1_RL, rfMRI_REST2_LR, and rfMRI_REST2_RL). Considering the susceptibility of time-frequency analysis to time samples, the four scans of each participant were amalgamated in the analysis (Honari et al., 2021; Wang et al., 2020). The study used surface-based CIFTI resting-state fMRI scans (MSMall registered) that had undergone prior pre-processing with the HCP's ICA-based artifact removal process, in order to minimize the effects of spatially structured noise. All brain imaging data were procured on a custom Siemens 3T Skyra at Washington University in St. Louis using a multi-band sequence. Structural images were captured at a 0.7-mm isotropic resolution, while the resting-state fMRI data had a 2-mm isotropic spatial resolution and a TR of 0.72 s. Informed consent was obtained from all participants, with all methods conforming to relevant guidelines. The 3T task data were excluded from the analysis due to their limited scan duration (3 to 5 min), as the objective was to investigate the very slow frequency bands.

In correspondence with the 3T resting-state data, the 7T resting-state data included four 16-minute scans per participant (rfMRI_REST1_PA, rfMRI_REST2_AP, rfMRI_REST3_PA, and rfMRI_REST4_AP). The 7T task data included movie watching and retinotopy. Movie-watching data was incorporated, given its approximately 15-min scan duration. Each movie-watching scan consists of several clips with separated by 20-s rest periods (details are available in WU–Minn HCP S1200 Release Reference Manual). CIFTI fMRI scans that underwent ICA-based artifact removal were utilized, mirroring the 3T data selection. These data were collected at a resolution of 1.6-mm isotropic and 1-second TR, utilizing a multi-band acceleration of 5, in-plane acceleration of 2, and 85 slices.

4.2. Preprocessing

The data used in this study have already undergone the HCP ICA-based denoising, negating the need for further preprocessing (Bolt et al., 2022; Raut et al., 2021; Van Essen et al., 2013; Zhang et al., 2020). For all fMRI scans, the signals from brain regions were extracted using the HCP-MMP 1.0 template and the activity of vertices inside each of the 360 regions was averaged to get 1 time series per region (Glasser et al., 2016). Subsequently, the signals from each region were filtered to the 0.01–0.1 Hz range using a zero-phase filter ("filtfilt" function in MATLAB), consistent with previous fMRI phase studies (Bolt et al., 2022; Honari et al., 2021).

4.3. Peak frequency

The rate of phase change can be characterized as the PF, which can be calculated by the first derivative of the phase angle time series. Higher PF corresponds to faster phase angle variation. This technique was originally developed for measuring the frequency fluctuation of EEG signals by Cohen (2014), who coined the term "frequency sliding" (Cohen, 2014). We adapt this method to low-frequency fMRI signals as the methodology depicted in Fig. 1.

We first applied a zero-phase filter to the raw BOLD signal (step 1) to yield a filtered signal without phase distortion (step 2), as recommended by a prior fMRI study on phase (Honari et al., 2021; Pedersen et al., 2018). Previous fMRI phase studies have advocated narrow-band filtering to satisfy Bedrosian's theorem and generate meaningful envelopes and phases of an analytic signal (Pedersen et al., 2018). In our pursuit to examine frequencies from slow to fast, we divided the signal into four narrow sub-bands: 0.01–0.03 Hz, 0.03–0.05 Hz, 0.05–0.07 Hz, and 0.07–0.09 Hz. We then applied the Hilbert transform to obtain the analytic representation and extract the phase angle time series, as given by the following equation (step 3):

$$z(t) = y(t) + j\widetilde{y}(t) = a(t)e^{j\varphi(t)} \quad (1)$$

where $j = \sqrt{-1}$, $\widetilde{y}$ denotes the Hilbert transform of y, $a(t)$ denote amplitudes and $\varphi(t)$ denote phases of signal $z(t)$. Upon calculating the first derivative of the phase angle time series, we applied a median filter using MATLAB's "medfilt" function to the derivative time series to mitigate large "blips" and negative derivatives due to jumps in the unwrapped phase angle time series. Given that fMRI data comprise fewer time points than EEG data, we increased the median filter order from 10 (used in EEG) to 20 to counteract larger phase jumps in BOLD signal (step 4). To discern phase-specific PF, we calculated the mean PF within a narrow phase window (e.g., a peak is defined from -π/12–π/12 or -15°–15°).

To rule out the edge effect that may be caused by the 0.01–0.03 Hz filtering, the same analysis is done for 0.005–0.01 Hz within 0.005–0.1 Hz band-pass filtering.

4.4. Validation on Lechner and Northoff (2023) method

The Frequency Sliding Method, initially conceived for high-frequency EEG/MEG analysis, is deployed for the first time on fMRI data in this study. In an endeavor to assess its replicability, we explored its congruence with the recently formulated Lechner and Northoff (2023) method. The Lechner and Northoff (2023) method has been developed to measure the stability of phase dynamics. It designates the -π as the commencement point for each cycle. It computes the time delays from the starting point of a given cycle to the starting points of the successor cycle, subsequently forming a series corresponding to each cycle duration. We further assessed the spatial similarity between the average of PF and cycle duration across the entire time series for each brain region.

4.5. Phase cycle modulation on PF

We employed the normalized Kullback-Leibler (KL) divergence of PF distribution P on each phase cycle against a uniform distribution Q to quantify the phase modulation effect on PF. To scrutinize fine-grained phases, phases from -180° to 180° were binned into 360 windows, each with a length of 30° and a step length of 1°. Hence, the cycle of phase is divided into -180° to -150°, -179° to -149°, -178° to -148°, and so forth. As a result, we obtained 360 values of PF at each phase cycle. The probability distribution of PF is given by the following equation:

$$P_{PF} = \frac{PF(\phi)}{\sum PF(\phi)}$$

where $PF(\phi)$ represents the value of PF at phase ϕ degree. Subsequently, Shannon entropy was calculated, which reflects the quantity of information for a distribution. If a time series is highly predictable, Shannon entropy will be lower; If a time series is uniformly distributed and hence unpredictable, Shannon entropy is maximal. Shannon entropy of PF is calculated as the equation below:

$$H(P) = -\sum_{j=1}^{N} P_{PF}(j) log P_{PF}(j)$$

where N is the length of the total phase bins. $Log(N)$ is the maximal entropy of a distribution, corresponding to a uniform distribution. The KL divergence is calculated by the following equation:

$$D_{KL}(P_{PF}, Q) = Log(N) - H(P)$$

Since the uniform distribution is represented by $Log(N)$, we normalized the KL divergence by the following equation:

$$D_{KL\ norm.}(P_{PF}, Q) = \frac{D_{KL}(P_{PF}, Q)}{Log(N)}$$

This definition of normalized KL divergence aligns with previous studies, which used it to examine cross-frequency phase modulation on amplitude (Tort et al., 2010) or behavioral reaction (Helfrich et al., 2018).

4.6. Autocorrelation window (ACW)

The autocorrelation functions for time courses of the 360 regions were calculated using MATLAB's "autocorr" function. The ACW value was subsequently defined as the first lag at which the autocorrelation diminishes to zero within the infraslow frequency range (0.01–0.1 Hz), consistent with prior studies (Golesorkhi et al., 2021a; Ito et al., 2020; Raut et al., 2020). It is important to note that we did not assess ACW across the four narrow bands corresponding to the PF calculations. This decision is grounded in the understanding that ACW represents the neural temporal receptive window, reflecting the duration over which neural activity returns to its baseline (Golesorkhi et al., 2021a). In line with this concept, the INT should encompass a broad spectrum of neural signal timescales, rather than being restricted to a specific frequency band (Golesorkhi et al., 2021b). To maintain data transparency, we have illustrated the ACW topography for these four narrow bands in Supplementary Fig. 1. As narrowband filtering imposes a fixed timescale on the neural signal, it revealed topographies with less variability across regions. Moreover, the constrained temporal resolution of fMRI limits the computation of ACW in higher frequency narrow bands due to the scarcity of time samples, leading to a uniform distribution of ACW across different regions (see 0.07–0.09 Hz Supplementary Fig. 1).

4.7. Spatial similarity

We evaluated the similarity between PF and ACW using spatial correlation. Initially, brain maps of PF and ACW were z-scored on an individual basis. Subsequently, spatial similarity was calculated as a single Pearson's correlation coefficient between PF and ACW topographical maps across brain regions. This calculation was performed after averaging across subjects, thereby generating a single brain per condition (Golesorkhi et al., 2021a; Wang et al., 2018).

We further examined the correlation between ACW and non-phase-based frequency power (Cohen, 2014). The phase information of PF, i.e., its phase angle, captures the non-linear properties of a signal (Cohen, 2014; Glerean et al., 2012; Laird et al., 2002), while these nonlinear properties are eliminated when calculating frequency power (Hua et al., 2022). In the case of frequency power, the analysis paralleled that of PF, with one distinction: frequency power involves extracting the modulus of the Hilbert transform, thereby reflecting the amplitude/power of a frequency band based on its linearity (Cohen, 2014). We calculated the frequency power across our four sub-frequency bands as a linear measurement, and evaluated its correlation with ACW relative to PF, to investigate which metric exhibits greater correlation with INT.

4.8. Surrogate data examination

To estimate the influence of phase modulation on PF and the similarity between PF and ACW under the null hypothesis of a linear and Gaussian stationary stochastic process (Chang and Glover, 2010; Liégeois et al., 2021; Zalesky et al., 2014), we employed surrogate data generated by shuffling the Fourier phases. This method manipulates only the phase information of a signal while preserving its amplitude/power spectrum characteristics (Schreiber and Schmitz, 2000). The process begins with the application of a Fourier transform to the time-series data, converting it to the frequency domain. Subsequently, the timings of the signal's phases are randomized independently across each frequency component. Following this phase randomization, an inverse Fourier transform is applied, reconverting the data back to the time domain. In our study, the time series data from various regions, sessions, and individuals in the actual dataset were each shuffled to generate a surrogate dataset that mirrors the original in the phase structure albeit shifted along the time points.

4.9. Statistics

Given that the same subjects were included in both the 3T and 7T resting-state and task-state data, we conducted a 4-by-4 within-subject ANOVA for PF in four sub-bands (0.01–0.03 Hz, 0.03–0.05 Hz, 0.05–0.07 Hz, and 0.07–0.09 Hz) and for four phases [peak (-15°∼15°), trough (165°∼180°&-180°∼-165°), rise (-105°∼-75°), and fall (75°∼105°)]. A one-way ANOVA was applied for the KL divergence in the four sub-bands. All post-hoc tests were conducted using two-tailed *t*-tests. Additionally, we assessed the correlations of R values using two-tailed *z*-tests. Furthermore, all multiple comparisons—including those of brain regions, frequencies, and phases—were corrected using the False Discovery Rate (FDR) criterion.

Ethics statement

The MRI datasets used in this study are from the Human Connectome Project (https://db.humanconnectome.org). The HCP scanning protocol was approved by the local Institutional Review Board at Washington University in St. Louis.

CRediT authorship contribution statement

Yujia Ao: Conceptualization, Data curation, Formal analysis, Investigation, Methodology, Software, Validation, Visualization, Writing – original draft, Writing – review & editing. **Yasir Catal:** Software, Validation, Writing – review & editing. **Stephan Lechner:** Software, Validation, Writing – review & editing. **Jingyu Hua:** Validation, Writing – review & editing. **Georg Northoff:** Conceptualization, Investigation, Methodology, Project administration, Resources, Supervision, Validation, Writing – review & editing.

Declaration of Competing Interest

The authors declare that the research was conducted in the absence of any commercial or financial relationships that could be construed as a potential conflict of interest.

Data availability

The data that support the findings of this study are available at the Human Connectome Project's repository at https://db.humanconnectome.org.

Acknowledgments

This research has received funding from the European Union's Horizon 2020 Framework Program for Research and Innovation under the Specific Grant Agreement no, 785907 (Human Brain Project SGA2). Y.A. is grateful for the support by China Scholarship Council (202208510069). G.N. is grateful for funding provided by UMRF, uOBMRI, CIHR and PSI. We are also grateful to CIHR, NSERC, and SSHRC for supporting our tri-council grant from the Canada–UK Artificial Intelligence (AI) Initiative The self as agent–environment nexus: crossing disciplinary boundaries to help human selves and anticipate artificial selves' (ES/T01279X/1) (together with Karl J. Friston from the UK).

Supplementary materials

Supplementary material associated with this article can be found, in the online version, at doi:10.1016/j.neuroimage.2023.120482.

References

Adaikkan, C., Middleton, S.J., Marco, A., Pao, P.C., Mathys, H., Kim, D.N.W., Gao, F., Young, J.Z., Suk, H.J., Boyden, E.S., McHugh, T.J., Tsai, L.H., 2019. Gamma entrainment binds higher-order brain regions and offers neuroprotection. Neuron 102 (5), 929–943. https://www.ncbi.nlm.nih.gov/pmc/articles/PMC6697125/pdf/nihms-1528873.pdf.

Alderson, T.H., Bokde, A.L., Kelso, J.S., Maguire, L., Coyle, D., 2020. Metastable neural dynamics underlies cognitive performance across multiple behavioural paradigms. Hum. Brain Mapp. 41 (12), 3212–3234. https://doi.org/10.1002/hbm.25009.

Ao, Y., Kou, J., Yang, C., Wang, Y., Huang, L., Jing, X., Cui, Q., Cai, X., Chen, J., 2022. The temporal dedifferentiation of global brain signal fluctuations during human brain ageing. Sci. Rep. 12 (1), 3616 https://doi.org/10.1038/s41598-022-07578-6.

Ao, Y., Yang, C., Drewes, J., Jiang, M., Huang, L., Jing, X., Northoff, G., Wang, Y., 2023. Spatiotemporal dedifferentiation of the global brain signal topography along the adult lifespan. Hum. Brain Mapp. 44 (17), 5906–5918. https://doi.org/10.1002/hbm.26484.

Benwell, C.S.Y., London, R.E., Tagliabue, C.F., Veniero, D., Gross, J., Keitel, C., Thut, G., 2019. Frequency and power of human alpha oscillations drift systematically with time-on-task. Neuroimage 192, 101–114. https://doi.org/10.1016/j.neuroimage.2019.02.067.

Bolt, T., Nomi, J.S., Bzdok, D., Salas, J.A., Chang, C., Thomas Yeo, B.T., Uddin, L.Q., Keilholz, S.D., 2022. A parsimonious description of global functional brain organization in three spatiotemporal patterns. Nat. Neurosci. 25 (8), 1093–1103. https://doi.org/10.1038/s41593-022-01118-1.

Buccellato, A., Zang, D., Zilio, F., Gomez-Pilar, J., Wang, Z., Qi, Z., Zheng, R., Xu, Z., Wu, X., Bisiacchi, P., 2023. Disrupted relationship between intrinsic neural timescales and alpha peak frequency during unconscious states—A high-density EEG study. Neuroimage 265, 119802. https://doi.org/10.1016/j.neuroimage.2022.119802.

Buzsaki, G., Draguhn, A., 2004. Neuronal oscillations in cortical networks. Science 304 (5679), 1926–1929. https://doi.org/10.1126/science.1099745.

Buzsáki, G., Draguhn, A., 2004. Neuronal oscillations in cortical networks. Science 304 (5679), 1926–1929. https://doi.org/10.1126/science.1099745.

Chang, C., Glover, G.H., 2010. Time-frequency dynamics of resting-state brain connectivity measured with fMRI. Neuroimage 50 (1), 81–98.

Chen, J.E., Glover, G.H., 2015. BOLD fractional contribution to resting-state functional connectivity above 0.1 Hz. Neuroimage 107, 207–218.

Cohen, M.X., 2014. Fluctuations in oscillation frequency control spike timing and coordinate neural networks. J. Neurosci. 34 (27), 8988–8998. https://doi.org/10.1523/JNEUROSCI.0261-14.2014.

Demirtaş, M., Ponce-Alvarez, A., Gilson, M., Hagmann, P., Mantini, D., Betti, V., Romani, G.L., Friston, K., Corbetta, M., Deco, G., 2019. Distinct modes of functional connectivity induced by movie-watching. Neuroimage 184, 335–348.

Doucet, G., Naveau, M., Petit, L., Zago, L., Crivello, F., Jobard, G., Delcroix, N., Mellet, E., Tzourio-Mazoyer, N., Mazoyer, B., 2012. Patterns of hemodynamic low-frequency oscillations in the brain are modulated by the nature of free thought during rest. Neuroimage 59 (4), 3194–3200.

Finn, E.S., Bandettini, P.A., 2021. Movie-watching outperforms rest for functional connectivity-based prediction of behavior. Neuroimage 235, 117963.

Garrett, D.D., Samanez-Larkin, G.R., MacDonald, S.W., Lindenberger, U., McIntosh, A.R., Grady, C.L., 2013. Moment-to-moment brain signal variability: a next frontier in human brain mapping? Neurosci. Biobehav. Rev. 37 (4), 610–624. https://doi.org/10.1016/j.neubiorev.2013.02.015.

Glasser, M.F., Coalson, T.S., Robinson, E.C., Hacker, C.D., Harwell, J., Yacoub, E., Ugurbil, K., Andersson, J., Beckmann, C.F., Jenkinson, M., Smith, S.M., Van Essen, D. C., 2016. A multi-modal parcellation of human cerebral cortex. Nature 536 (7615), 171–178. https://doi.org/10.1038/nature18933.

Glerean, E., Salmi, J., Lahnakoski, J.M., Jääskeläinen, I.P., Sams, M., 2012. Functional magnetic resonance imaging phase synchronization as a measure of dynamic functional connectivity. Brain Connect 2 (2), 91–101.

Golesorkhi, M., Gomez-Pilar, J., Tumati, S., Fraser, M., Northoff, G., 2021a. Temporal hierarchy of intrinsic neural timescales converges with spatial core-periphery organization. Commun. Biol. 4 (1), 277. https://doi.org/10.1038/s42003-021-01785-z.

Golesorkhi, M., Gomez-Pilar, J., Zilio, F., Berberian, N., Wolff, A., Yagoub, M.C.E., Northoff, G., 2021b. The brain and its time: intrinsic neural timescales are key for input processing. Commun. Biol. 4 (1), 970. https://doi.org/10.1038/s42003-021-02483-6.

Gong, Z.-Q., Zuo, X.-N., 2023. Connectivity gradients in spontaneous brain activity at multiple frequency bands. Cereb. Cortex 33 (17), 9718–9728.

Gu, Y., Sainburg, L.E., Kuang, S., Han, F., Williams, J.W., Liu, Y., Zhang, N., Zhang, X., Leopold, D.A., Liu, X., 2021. Brain activity fluctuations propagate as waves traversing the cortical hierarchy. Cereb. Cortex 31 (9), 3986–4005. https://doi.org/10.1093/cercor/bhab064.

Gutierrez-Barragan, D., Basson, M.A., Panzeri, S., Gozzi, A., 2019. Infraslow state fluctuations govern spontaneous fMRI network dynamics. Curr. Biol. 29 (14), 2295–2306. https://doi.org/10.1016/j.cub.2019.06.017.

Gutierrez-Barragan, D., Singh, N.A., Alvino, F.G., Coletta, L., Rocchi, F., De Guzman, E., Galbusera, A., Uboldi, M., Panzeri, S., Gozzi, A., 2022. Unique spatiotemporal fMRI dynamics in the awake mouse brain. Curr. Biol. 32 (3), 631–644. https://doi.org/10.1016/j.cub.2021.12.015.

Han, Y., Wang, J., Zhao, Z., Min, B., Lu, J., Li, K., He, Y., Jia, J., 2011. Frequency-dependent changes in the amplitude of low-frequency fluctuations in amnestic mild cognitive impairment: a resting-state fMRI study. Neuroimage 55 (1), 287–295. https://doi.org/10.1016/j.neuroimage.2010.11.059.

Hasson, U., Chen, J., Honey, C.J., 2015. Hierarchical process memory: memory as an integral component of information processing. Trends Cogn. Sci. 19 (6), 304–313. https://doi.org/10.1016/j.tics.2015.04.006.

Helfrich, R.F., Fiebelkorn, I.C., Szczepanski, S.M., Lin, J.J., Parvizi, J., Knight, R.T., Kastner, S., 2018. Neural mechanisms of sustained attention are rhythmic. Neuron 99 (4), 854–865. https://doi.org/10.1016/j.neuron.2018.07.032 e855.

Himberger, K.D., Chien, H.-Y., Honey, C.J., 2018. Principles of temporal processing across the cortical hierarchy. Neuroscience 389, 161–174. https://doi.org/10.1016/j.neuroscience.2018.04.030.

Honari, H., Choe, A.S., Lindquist, M.A., 2021. Evaluating phase synchronization methods in fMRI: a comparison study and new approaches. Neuroimage 228, 117704. https://doi.org/10.1016/j.neuroimage.2020.117704.

Honey, C.J., Thesen, T., Donner, T.H., Silbert, L.J., Carlson, C.E., Devinsky, O., Doyle, W. K., Rubin, N., Heeger, D.J., Hasson, U., 2012. Slow cortical dynamics and the accumulation of information over long timescales. Neuron 76 (2), 423–434. https://doi.org/10.1016/j.neuron.2012.08.011.

Hua, J., Wolff, A., Zhang, J., Yao, L., Zang, Y., Luo, J., Ge, X., Liu, C., Northoff, G., 2022. Alpha and theta peak frequency track on-and off-thoughts. Commun. Biol. 5 (1), 209. https://doi.org/10.1038/s42003-022-03146-w.

Huang, Z., Dai, R., Wu, X., Yang, Z., Liu, D., Hu, J., Gao, L., Tang, W., Mao, Y., Jin, Y., 2014. The self and its resting state in consciousness: an investigation of the vegetative state. Hum. Brain Mapp. 35 (5), 1997–2008.

Huang, Z., Zhang, J., Longtin, A., Dumont, G., Duncan, N.W., Pokorny, J., Qin, P., Dai, R., Ferri, F., Weng, X., Northoff, G., 2017. Is there a nonadditive interaction between spontaneous and evoked activity? Phase-dependence and its relation to the temporal structure of scale-free brain activity. Cereb. Cortex 27 (2), 1037–1059. https://doi.org/10.1093/cercor/bhv288.

Huk, A., Bonnen, K., He, B.J., 2018. Beyond trial-based paradigms: continuous behavior, ongoing neural activity, and natural stimuli. J. Neurosci. 38 (35), 7551–7558.

Huntenburg, J.M., Bazin, P.L., Margulies, D.S., 2018. Large-scale gradients in human cortical organization. Trends Cogn. Sci. 22 (1), 21–31. https://doi.org/10.1016/j.tics.2017.11.002.

Ito, T., Hearne, L.J., Cole, M.W., 2020. A cortical hierarchy of localized and distributed processes revealed via dissociation of task activations, connectivity changes, and intrinsic timescales. Neuroimage 221, 117141. https://doi.org/10.1016/j.neuroimage.2020.117141.

Klimesch, W., Sauseng, P., Hanslmayr, S., 2007. EEG alpha oscillations: the inhibition-timing hypothesis. Brain Res. Rev. 53 (1), 63–88. https://doi.org/10.1016/j.brainresrev.2006.06.003.

Kringelbach, M.L., Deco, G., 2020. Brain states and transitions: insights from computational neuroscience. Cell Rep. 32 (10), 108128 https://doi.org/10.1016/j.celrep.2020.108128.

Kringelbach, M.L., Perl, Y.S., Tagliazucchi, E., Deco, G., 2023. Toward naturalistic neuroscience: mechanisms underlying the flattening of brain hierarchy in movie-watching compared to rest and task. Sci. Adv. 9 (2), eade6049. https://doi.org/10.1126/sciadv.ade6049.

Laird, A.R., Rogers, B.P., Carew, J.D., Arfanakis, K., Moritz, C.H., Meyerand, M.E., 2002. Characterizing instantaneous phase relationships in whole-brain fMRI activation data. Hum. Brain Mapp. 16 (2), 71–80.

Lechner, S., Northoff, G., 2023. Temporal imprecision and phase instability in schizophrenia resting state EEG. Asian J. Psychiatry, 103654. https://doi.org/10.1016/j.ajp.2023.103654.

Liégeois, R., Yeo, B.T., Van De Ville, D., 2021. Interpreting null models of resting-state functional MRI dynamics: not throwing the model out with the hypothesis. Neuroimage 243, 118518.

Margulies, D.S., Ghosh, S.S., Goulas, A., Falkiewicz, M., Huntenburg, J.M., Langs, G., Bezgin, G., Eickhoff, S.B., Castellanos, F.X., Petrides, M., Jefferies, E., Smallwood, J., 2016. Situating the default-mode network along a principal gradient of macroscale cortical organization. Proc. Natl. Acad. Sci. USA 113 (44), 12574–12579. https://doi.org/10.1073/pnas.1608282113.

Northoff, G., Huang, Z., 2017. How do the brain's time and space mediate consciousness and its different dimensions? Temporo-spatial theory of consciousness (TTC). Neurosci. Biobehav. Rev. 80, 630–645. https://doi.org/10.1016/j.neubiorev.2017.07.013.

Northoff, G., Wainio-Theberge, S., Evers, K., 2020a. Is temporo-spatial dynamics the "common currency" of brain and mind? In quest of "spatiotemporal neuroscience". Phys. Life Rev. 33, 34–54. https://doi.org/10.1016/j.plrev.2019.05.002.

Northoff, G., Wainio-Theberge, S., Evers, K., 2020b. Spatiotemporal neuroscience—what is it and why we need it. Phys. Life Rev. 33, 78–87. https://doi.org/10.1016/j.plrev.2020.06.005.

Palva, J.M., Palva, S., 2012. Infra-slow fluctuations in electrophysiological recordings, blood-oxygenation-level-dependent signals, and psychophysical time series. Neuroimage 62 (4), 2201–2211.

Palva, S., Palva, J.M., 2018. Roles of brain criticality and multiscale oscillations in temporal predictions for sensorimotor processing. Trends Neurosci. 41 (10), 729–743. https://doi.org/10.1016/j.tins.2018.08.008.

Pang, J.C., Aquino, K.M., Oldehinkel, M., Robinson, P.A., Fulcher, B.D., Breakspear, M., Fornito, A., 2023. Geometric constraints on human brain function. Nature 1–9. https://doi.org/10.1038/s41586-023-06098-1.

Pang, J.C., Gollo, L.L., Roberts, J.A., 2021. Stochastic synchronization of dynamics on the human connectome. Neuroimage 229, 117738. https://doi.org/10.1016/j.neuroimage.2021.117738.

Pedersen, M., Omidvarnia, A., Zalesky, A., Jackson, G.D., 2018. On the relationship between instantaneous phase synchrony and correlation-based sliding windows for time-resolved fMRI connectivity analysis. Neuroimage 181, 85–94. https://doi.org/10.1016/j.neuroimage.2018.06.020.

Rajimehr, R., Xu, H., Farahani, A., Kornblith, S., Duncan, J., Desimone, R., 2022. Functional architecture of cerebral cortex during naturalistic movie-watching. BioRxiv. https://doi.org/10.1101/2022.03.14.483878, 2022.2003.2014.483878.

Raut, R.V., Mitra, A., Marek, S., Ortega, M., Snyder, A.Z., Tanenbaum, A., Laumann, T.O., Dosenbach, N.U., Raichle, M.E., 2020a. Organization of propagated intrinsic brain activity in individual humans. Cereb. Cortex 30 (3), 1716–1734. https://doi.org/10.1093/cercor/bhz198.

Raut, R.V., Snyder, A.Z., Mitra, A., Yellin, D., Fujii, N., Malach, R., Raichle, M.E., 2021. Global waves synchronize the brain's functional systems with fluctuating arousal. Sci. Adv. 7 (30), eabf2709. https://doi.org/10.1126/sciadv.abf2709.

Raut, R.V., Snyder, A.Z., Raichle, M.E., 2020b. Hierarchical dynamics as a macroscopic organizing principle of the human brain. Proc. Natl. Acad. Sci. 117 (34), 20890–20897. https://doi.org/10.1073/pnas.2003383117.

Samaha, J., Postle, B.R., 2015. The speed of alpha-band oscillations predicts the temporal resolution of visual perception. Curr. Biol. 25 (22), 2985–2990. https://doi.org/10.1016/j.cub.2015.10.007.

Sasai, S., Koike, T., Sugawara, S.K., Hamano, Y.H., Sumiya, M., Okazaki, S., Takahashi, H.K., Taga, G., Sadato, N., 2021. Frequency-specific task modulation of human brain functional networks: a fast fMRI study. Neuroimage 224, 117375. https://doi.org/10.1016/j.neuroimage.2020.117375.

Scalabrini, A., Vai, B., Poletti, S., Damiani, S., Mucci, C., Colombo, C., Zanardi, R., Benedetti, F., Northoff, G., 2020. All roads lead to the default-mode network-global source of DMN abnormalities in major depressive disorder. Neuropsychopharmacology 45 (12), 2058–2069. https://doi.org/10.1038/s41386-020-0785-x.

Scheinost, D., Tokoglu, F., Shen, X., Finn, E.S., Noble, S., Papademetris, X., Constable, R. T., 2016. Fluctuations in global brain activity are associated with changes in whole-brain connectivity of functional networks. IEEE Trans. Biomed. Eng. 63 (12), 2540–2549. https://doi.org/10.1109/TBME.2016.2600248.

Schreiber, T., Schmitz, A., 2000. Surrogate time series. Physica D 142 (3–4), 346–382.

Shine, J.M., Bissett, P.G., Bell, P.T., Koyejo, O., Balsters, J.H., Gorgolewski, K.J., Moodie, C.A., Poldrack, R.A., 2016. The dynamics of functional brain networks: integrated network states during cognitive task performance. Neuron 92 (2), 544–554. https://doi.org/10.1016/j.neuron.2016.09.018.

Stark, E.A., Cabral, J., Riem, M.M., Van IJzendoorn, M.H., Stein, A., Kringelbach, M.L., 2020. The power of smiling: the adult brain networks underlying learned infant emotionality. Cereb. Cortex 30 (4), 2019–2029. https://doi.org/10.1093/cercor/bhz219.

Thompson, W.H., Fransson, P., 2015. The frequency dimension of fMRI dynamic connectivity: network connectivity, functional hubs and integration in the resting brain. Neuroimage 121, 227–242.

Tort, A.B., Komorowski, R., Eichenbaum, H., Kopell, N., 2010. Measuring phase-amplitude coupling between neuronal oscillations of different frequencies. J. Neurophysiol. 104 (2), 1195–1210. https://doi.org/10.1152/jn.00106.2010.

Van Essen, D.C., Smith, S.M., Barch, D.M., Behrens, T.E., Yacoub, E., Ugurbil, K., Consortium, W.U.-M.H., 2013. The WU–Minn human connectome project: an overview. Neuroimage 80, 62–79. https://doi.org/10.1016/j.neuroimage.2013.05.041.

Wang, Y., Chen, W., Ye, L., Biswal, B.B., Yang, X., Zou, Q., Yang, P., Yang, Q., Wang, X., Cui, Q., Duan, X., Liao, W., Chen, H., 2018. Multiscale energy reallocation during low-frequency steady-state brain response. Hum. Brain Mapp. 39, 2121–2132. https://doi.org/10.1002/hbm.23992.

Wang, Y., Huang, X., Yang, X., Yang, Q., Wang, X., Northoff, G., Pang, Y., Wang, C., Cui, Q., Chen, H., 2019. Low-frequency phase-locking of brain signals contribute to efficient face recognition. Neuroscience 422, 172–183. https://doi.org/10.1016/j.neuroscience.2019.10.024.

Wang, Y., Zou, Q., Ao, Y., Liu, Y., Ouyang, Y., Wang, X., Biswal, B., Cui, Q., Chen, H., 2020. Frequency-dependent circuits anchored in the dorsal and ventral left anterior insula. Sci. Rep. 10 (1), 16394. https://doi.org/10.1038/s41598-020-73192-z.

Wolff, A., Berberian, N., Golesorkhi, M., Gomez-Pilar, J., Zilio, F., Northoff, G., 2022. Intrinsic neural timescales: temporal integration and segregation. Trends Cogn. Sci. 26 (2), 159–173. https://doi.org/10.1016/j.tics.2021.11.007.

Wolff, A., de la Salle, S., Sorgini, A., Lynn, E., Blier, P., Knott, V., Northoff, G., 2019. Atypical temporal dynamics of resting state shapes stimulus-evoked activity in depression-an EEG study on rest-stimulus interaction. Front. Psychiatry 10, 719. https://doi.org/10.3389/fpsyt.2019.00719.

Wolman, A., Çatal, Y., Wolff, A., Wainio-Theberge, S., Scalabrini, A., El Ahmadi, A., Northoff, G., 2023. Intrinsic neural timescales mediate the cognitive bias of self–temporal integration as key mechanism. Neuroimage 268, 119896. https://doi.org/10.1016/j.neuroimage.2023.119896.

Wutz, A., Melcher, D., Samaha, J., 2018. Frequency modulation of neural oscillations according to visual task demands. Proc. Natl. Acad. Sci. 115 (6), 1346–1351. https://doi.org/10.1073/pnas.1713318115.

Yeshurun, Y., Nguyen, M., Hasson, U., 2021. The default mode network: where the idiosyncratic self meets the shared social world. Nat. Rev. Neurosci. 22 (3), 181–192. https://doi.org/10.1038/s41583-020-00420-w.

Zalesky, A., Fornito, A., Cocchi, L., Gollo, L.L., Breakspear, M., 2014. Time-resolved resting-state brain networks. Proc. Natl. Acad. Sci. 111 (28), 10341–10346.

Zhang, H., Yang, S.Y., Qiao, Y., Ge, Q., Tang, Y.Y., Northoff, G., Zang, Y.F., 2022. Default mode network mediates low-frequency fluctuations in brain activity and behavior during sustained attention. Hum. Brain Mapp. 43 (18), 5478–5489.

Zhang, J., Huang, Z., Tumati, S., Northoff, G., 2020. Rest-task modulation of fMRI-derived global signal topography is mediated by transient coactivation patterns. PLoS Biol. 18 (7), e3000733 https://doi.org/10.1371/journal.pbio.3000733.

Zilio, F., Gomez-Pilar, J., Cao, S., Zhang, J., Zang, D., Qi, Z., Tan, J., Hiromi, T., Wu, X., Fogel, S., 2021. Are intrinsic neural timescales related to sensory processing? Evidence from abnormal behavioral states. Neuroimage 226, 117579. https://doi.org/10.1016/j.neuroimage.2020.117579.

Zuo, X.N., Di Martino, A., Kelly, C., Shehzad, Z.E., Gee, D.G., Klein, D.F., Castellanos, F. X., Biswal, B.B., Milham, M.P., 2010. The oscillating brain: complex and reliable. Neuroimage 49 (2), 1432–1445. https://doi.org/10.1016/j.neuroimage.2009.09.037.